Article

Serum Pharmacochemistry Combined with Network Pharmacology-Based Mechanism Prediction and Pharmacological Validation of Zhenwu Decoction on Alleviating Isoprenaline-Induced Heart Failure Injury in Rats

Ruiyu Li,[§] Lv Zhu,[§] Mengyao Wu, Chengtian Tao, Yang Lu, Yunyan Zhao, Xiaofeng Jiang, Chi Zhang,* and Li Wan*

Read Online

ACCESS | Metrics & More | Article Recommendations | Supporting Information

ABSTRACT: Zhenwu decoction (ZWD) is a famous classical formula in the treatment of heart failure (HF) with significant clinical effects. Owing to the complex material basis of ZWD, it is challenging to elucidate the pharmacodynamic substances and pharmacological mechanisms of ZWD against HF. Therefore, an ultrahigh-performance liquid chromatography system coupled with a high-resolution orbitrap mass spectrometry method was used to profile the chemical components and the absorbed prototype constituents in ISO-induced HF rat serum after oral administration of ZWD, and 33 out of 115 compounds were identified. In the *in vivo* study, ZWD could improve cardiac function and reduce the content of serum biochemical indexes, which are heart failure markers. With the help of network pharmacology and molecular docking simulation analysis, 112 ZWD targets oriented by HF were obtained, with STAT3, TNF, AKT1, VEGFA, and ALB as the core targets. Furthermore, we found that paeoniflorin and its derivatives may play a bigger role than other serum migrant components. Enriched pathway analysis yielded multiple HF-related signaling pathways, which indicated that ZWD may attenuate HF through the effect of PI3K-Akt, and MAPK pathways by regulating key targets such as STAT3, TNF, and AKT1. Finally, STAT3/MAPK pathways were experimentally validated in the anti-HF effect of ZWD. The phosphorylation levels of p38, JNK, ERK, and STAT3 were significantly increased in the ISO group and reversed by ZWD intervention. The results provided a reasonable strategy for the rapid screening of bioactive components in ZWD and a reference for quality control and further mechanism study of ZWD.
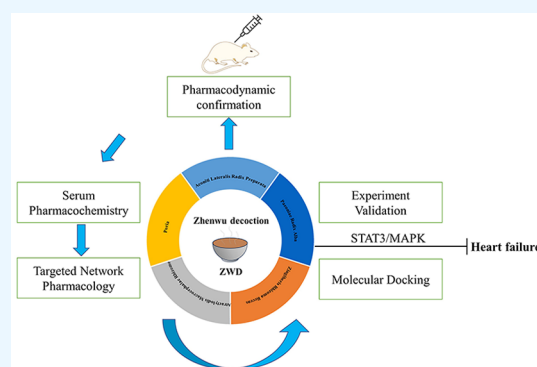
1. INTRODUCTION

Heart failure (HF) is a complex and chronic heart disease characterized by a declined capacity of the heart to pump or fill with blood, which is the last pathological process of many cardiovascular diseases. It has caused increasing morbidity and mortality rates in the elapsed decades.[1,2] The development of HF is typically preceded by pathological cardiac hypertrophy, which is usually characterized by an increase in the cardiomyocyte size and thickening of ventricular walls. When these changes become maladaptive, the heart ultimately fails.[3] Although tremendous progress has been made in the diagnosis and therapy of HF, no definitive methods still exist for treating HF.[4]

Traditional Chinese medicine (TCM) has been widely used to treat HF since long ago. It has provided a more accessible, flexible approach based on the abundant herb combinations created for different symptoms according to TCM theories. Zhenwu decoction (ZWD), a well-known classical TCM formula, was first described in *Treatise on Febrile Diseases*

written by Zhongjing Zhang and has almost 2000 years of clinical application history in China. It comprises Aconiti Lateralis Radix Preparata, Poria, Paeoniae Radix Alba, Zingiberis Rhizoma Recens, and Atractylodis Macrocephalae Rhizome. ZWD possesses various bioactivities such as anti-inflammation, antiapoptotic, neuroprotection, *etc.*[5−7] Modern research shows that ZWD has a therapeutic effect on HF, diabetic nephropathy, and other diseases.[8,9] However, only a few studies have investigated the mechanisms of ZWD in HF therapy, and the effective material remains unclear.

On the other hand, it is a well-acknowledged viewpoint that traditional Chinese medicinal herbs work through complex

interactions among complex disease targets and diverse chemical constituents.[10] However, this complexity makes it difficult to control the therapeutic effect and the quality of TCM. Also, it needs a reasonable and practical safety evaluation system, and it is relatively difficult to analyze its action and compatibility mechanism.[11]

To resolve the inherent complexity of TCM and give more acceptable aspects to understand TCM, numerous novel techniques and solutions have been proposed in the past few decades. Among them, serum pharmacochemistry and network pharmacology have been widely used to decipher the material basis and mechanism of TCM.[12,13] Serum pharmacochemistry of TCM is designed to screen the pharmacodynamic material basis of TCM from the constituents absorbed into the blood after oral administration, and these constituents were considered as the potential bioactive material basis of medicinal herbs.[14] Few studies of the serum pharmacochemistry of ZWD have been reported. The principle of network pharmacology was based on topology methods to analyze the "multi-component, multi-target, and multi-pathway" synergistic relationship between drugs, diseases, and targets.[15] It opens up a new field for the research of TCM. The fundamental idea of network pharmacology has much in common with the holistic view of TCM. It enables researchers to fully understand the efficacy and mechanism of multiple components in TCM from a holistic perspective.

Additionally, UHPLC-Q-Orbitrap-HRMS has become the most potent and reliable analytical technique for detecting and identifying chemical constituents in TCM or biological samples because of its high selectivity, high sensitivity, and effectivity.[16−18] This technique will undoubtedly help us to obtain more accurate information about the material basis of ZWD.

In this study, we successfully identified the chemical constituents of ZWD based on UHPLC-Q-Orbitrap-HRMS and integrated serum pharmacochemistry and network pharmacology to reveal the potential active components and potential mechanism of ZWD in HF rats.

2. MATERIALS AND METHODS

2.1. Materials and Reagents. Salsolinol, higenamine, aconine, neoline, benzoylmesaconine, benzoylaconine, benzoylhypaconine, hypaconitine, paeoniflorin, benzoylpaeoniflorin, 6-gingerol, atractylenolide III, and pachymic acid (the purity of reference standards was higher than 98%) were purchased from Chengdu Chroma-Biotechnology Co., Ltd. (Chengdu, China). Isoprenaline hydrochloride (ISO) was purchased from Shanghai Yien Chemical Technology Co., Ltd. (Shanghai, China). Captopril was obtained from Sinopharm Shantou Jinshi Pharmaceutical Co., Ltd. (Shantou, China). TNF-α, IL-6, BNP, and NT-Pro BNP Elisa kits were purchased from JingMei Biotechnology (Jiangsu, China). RIPA lysis buffer was from Meilun Biotechnology Co. Ltd. (Dalian, China) and the BCA protein kit was from Meilun Biotechnology Co. Ltd. (Dalian, China). Rabbit anti-p38, p-p38, JNK, p-JNK, ERK, p-ERK, STAT3, and p-STAT3 were from Cell Signaling Technology (Danvers). The ECL Western blot detection kit was from Meilun Biotechnology Co. Ltd. (Dalian, China). Acetonitrile and methanol (HPLC grade) were purchased from Fisher Scientific Co., Ltd. (Loughborough, UK), formic acid was purchased from Sigma-Aldrich (St. Louis, MO), and distilled water was purchased from Watsons Water Co., Ltd. (Shenzhen, China).

2.2. Zhenwu Decoction Water Extracts Preparation. The mixture of Aconiti Lateralis Radix Preparata (*Aconitum carmichaelii* Debx, Hei-Shun-Pian), Poria (*Poria cocos (Schw.)* Wolf, Fu-Ling), Paeoniae Radix Alba (*Paeonia lactiflora* Pall, Bai-Shao), Zingiberis Rhizoma Recens (*Zingiber officinale* Rosc, Sheng-Jiang), and Atractylodis Macrocephalae Rhizome (*Atractylodes macrocephala* Koidz, Bai-Zhu) (2.5:7:7:7:4.5) was soaked with 10 times volume distilled water for 30 min, heated, and maintained at boiling point for 144 min. The hot extraction was immediately filtered through a 100 mesh filter cloth. Finally, freeze-drying was carried out to obtain lyophilized powder, and the lyophilized powder yield was about 14%. The contents of paeoniflorin, 6-gingerol, and benzoylmesaconine were detected by HPLC. The detailed information is presented in Table S1. All herb materials were provided by China Resources Sanjiu (Yaan) Pharmaceutical Co., Ltd., and were tested and approved according to the Chinese Pharmacopoeia (2020 edition).

2.3. Qualitative Identification of Chemical Constituents and Serum Migrant Components (SMCs) of ZWD. *2.3.1. Preparation of Standard Solutions.* Salsolinol, higenamine, aconine, neoline, benzoylmesaconine, benzoylaconine, benzoylhypaconine, hypaconitine, paeoniflorin, benzoylpaeoniflorin, 6-gingerol, atractylenolide III, and pachymic acid were weighed and prepared with methanol to achieve the final concentration of 2.8, 2.9, 2.7, 2.6, 2.8, 2.7, 2.8, 3.1, 100.7, 100.8, 105.9, 100.7, and 100.8 μg/mL, respectively, to achieve a mixed standard solution, and kept at 4 °C before use.

2.3.2. Preparation of Sample Solutions. The ZWD water extracts (1g) acquired from section 2.2 were weighed and dissolved in 10 mL of 70% methanol. After vortexing for 5 min, the mixture solution was centrifuged at 13,000 rpm and maintained for 10 min, then the supernatant was filtered through a 0.22 μm membrane into a brown vial to obtain the sample solution.

The serum samples collected from section 2.4 were added with four times the volume of cold acetonitrile, made to stand for 10 min after vortexing, centrifuged at 12,000 rpm, and maintained for 10 min. Then, the supernatants were collected and dried with a nitrogen-blowing concentrator. The residues were dissolved with 300 μL of 70% methanol, and the centrifugation was repeated. Finally, the supernatant was filtered through a 0.22 μm membrane into the brown vial to obtain a serum solution.

2.3.3. Instrumentation and UHPLC-Q-Orbitrap-HRMS Conditions. The Vanquish UHPLC system (Thermo Fisher Scientific, United States) coupled with Q Exactive Quadrupole-Electrostatic Field Orbital Trap high-resolution mass spectrometry (UHPLC-Q-Orbitrap HRMS) was applied to analyze the ZWD water extracts and serum samples. Samples were separated using an ACQUITY UPLC HSS T3 C18 column (2.1 × 100 mm, 1.8 μm, Waters, United States). The mobile phase was deionized water with 0.1% formic acid (A) and acetonitrile (B). The gradient elution procedure was set as follows: 0−15 min, 10−100% B; 15−20 min, 100% B, 20−21 min, 100−10% B, 21−24 min, 10% B. The column temperature was maintained at 35 °C. The flow rate was set at 0.3 mL/min, and the injection volume was 2 μL.

All samples were detected in positive and negative ion modes through an ESI electrospray ion source by means of full scan/data-dependent secondary scan (Full MS/dd-MS2). MS parameters were set as follows: nitrogen was selected as the auxiliary gas and sheath gas. Auxiliary gas was 10 L/min and

sheath gas was 35 L/min with a spray voltage of 3 and −2.5 kV, respectively. The ion source temperature was kept at 320 °C. The auxiliary gas heating temperature was maintained at 350 °C. The primary resolution of the full scan was 70,000 with the scanning range from 100 to 1500 m/z. The secondary resolution was 17,500 with the collision energy gradient of 20, 40, and 60 eV, respectively.

2.3.4. Identification of Chemical Constituents. Compound Discoverer software 3.0 and Xcalibur 4.0 (Thermo Fisher Scientific) were applied to analyze the LC-MS raw data. Components were identified based on accurate molecular weight, the retention behaviors, and characteristics of ion adduction and fragmentation and compared to the databases (mz Cloud, mz Vault, ChemSpider, and PubChem). The mass deviation was less than 5 ppm. Finally, further confirmation was compared to the reference standards and the related literature.

2.4. Animals and Experimental Design. *2.4.1. Ethics Statement.* All *in vivo* experiments were carried out under the guidelines approved by the Institutional Animal Care and Use Committee (IACUC) of Chengdu University of Traditional Chinese Medicine (2021−50).

2.4.2. Animal and Experimental Groups. 40 Healthy Male Sprague−Dawley rats (weighing160−180 g, Specific Pathogen Free grade) were obtained from Beijing HFK Bioscience Co., Ltd. (Certification number: SCXK (Jing) 2019−0008). All rats were housed under standard conditions (50 ± 10% relative humidity, 12h light-dark cycle, 22 ± 2 °C) and allowed to eat and drink ad libitum. After adapting to the conditions for 1 week, rats were randomly divided into control, ISO, positive control, ZL + ISO, and ZH + ISO groups according to the body weight. The HF model was constructed according to a previous report.[19] Briefly, the rats in the ISO group were subcutaneously injected with isoprenaline hydrochloride 10 mg/kg/d for 2 weeks.

2.4.3. Experimental Drugs and Doses. After successfully establishing the model, the animals were administered intragastrically with low and high dosages of ZWD (6.1 and 24.5 g/kg/d, calculated in crude herbs) in the ZL + ISO group and ZH + ISO group separately. The adult dosage of ZWD is 116.8 g (crude drug) daily according to *Treatise on Febrile Diseases*. Based on the body surface area index, the rat dosage of ZWD is 12.26 g/kg daily. The low and high dosages of ZWD were calculated as 0.5 and 2 times of the rat daily dosage. In the positive control group, the animals were administered captopril 50 mg/kg/d through intragastric administration. The control group and ISO group were fed with equivalent distilled water. One week later, after the last drug administration, three rats were randomly selected from the ZH + ISO group and ISO group. The blood samples were obtained from the ophthalmic vein following anesthesia at 30, 60, 90, and 120 min and collected into the heparinized tubes and centrifuged at 4000 rpm and 4 °C for 10 min. The obtained supernatants were mixed, collected in clean dry tubes, and stored at −80 °C until serum migrant analysis.

At the fourth week, echocardiography, histopathology examinations, and the heart weight index were evaluated.

2.5. Echocardiography. At the fourth week, all experimental rats were anesthetized with 3% isoflurane, and 1.5% isoflurane was maintained by inhalation. Echocardiography measurements was conducted using a Vevo 3100 ultrahigh-resolution ultrasound system (FUJIFILM VisualSonics, Inc., Toronto, Ontario, Canada). The cardiac functions were recorded by five consecutive cardiac cycles on M-mode echocardiograms. Indicators such as ejection fraction (EF%), fractional shortening (FS%), left ventricular end-diastolic diameter (LVEDd), and left ventricular end-systolic diameter (LVESd) were calculated according to the Vevo 3100 software guidelines.

2.6. Assays of the Serum Biochemical Indexes. After echocardiography assessment, blood was taken from the abdominal aorta to obtain serum samples. The serum levels of AST, LDH, CK-MB, and α-HBDH were measured by an automatic chemistry analyzer (Mindary BS-240VET; Mindray Bio-Medical Electronics Co., Ltd., Shenzhen, China). TNF-α, IL-6, BNP, and NT-pro BNP were detected by an enzyme-linked immunosorbent assay and operated according to the experimental instructions.

2.7. Myocardial weight index and histology examination. The hearts were immediately removed and weighed after blood collection. Myocardial weight index was calculated by heart weight (HW) to body weight (BW). Then, the heart samples of all groups were fixed in 4% buffered formalin, which were subsequently dehydrated in gradient ethanol solution, cleared in xylene, and finally embedded in paraffin. The paraffin sections (3 μm) of heart tissues were stained with hematoxylin and eosin (H&E) for histological analysis and stained with Masson's trichrome for myocardial fibrosis evaluation. Collagen volume fraction (CVF%) was calculated using the Image-Pro Plus 6.0 software.

2.8. Targeted Network Pharmacology Analysis. *2.8.1. Target Acquisition of the Serum Migrant Components in Zhenwu Decoction against Heart Failure.* The SMCs that were targeted as potential effective ingredients were collected to screen potential treatment targets of ZWD against HF. Specifically, the SMCs were uploaded to various online servers and databases such as TCMSP (http://ibts.hkbu.edu.hk/LSP/tcmsp.php), Pharmmapper (http://www.lilab-ecust.cn/pharmmapper/), and Swiss target prediction (http://www.swisstargetprediction.ch/). "Heart Failure" was used as the keyword submitted to Comparative Toxicogenomics Database (CTD, http://ctdbase.org/), Therapeutic Target Database (TTD, http://db.idrblab.net/ttd/), Gene Cards (https://www.genecards.org/), and OMIM (https://omim.org/). Noteworthily, the disease targets in TTD and CTD marked "approved" or "marker/mechanism" and relevance score more than 10 in Gene Cards were further screened; the rest of the parameters were set as default. The targets collected were converted to standard gene names via the UniProt database (https://www.uniprot.org/). The duplicated, nonhuman, and nonstandard targets were eliminated. Then, the compound corresponding targets and disease targets were uploaded to Venn Diagrams (http://bioinformatics.psb.ugent.be/webtools/venn/) to obtain the common targets.

2.8.2. Construction of Serum Migrant Components—Predictive Target Network. To clarify and visualize the relationship between SMCs in ZWD and potential targets, the SMCs and common targets obtained from section 2.8.1 were rearranged to construct the compound-target network by using Cytoscape (3.9.1) software (https://cytoscape.org/). "Network Analyzer" plug-in was used to analyze the topology of the network. The size of the nodes reflected the size of the degree value in the network.

2.8.3. Protein−Protein Interaction (PPI) Network Construction. The common targets were integrated using the string platform (https://string-db.org/) to build its PPI and
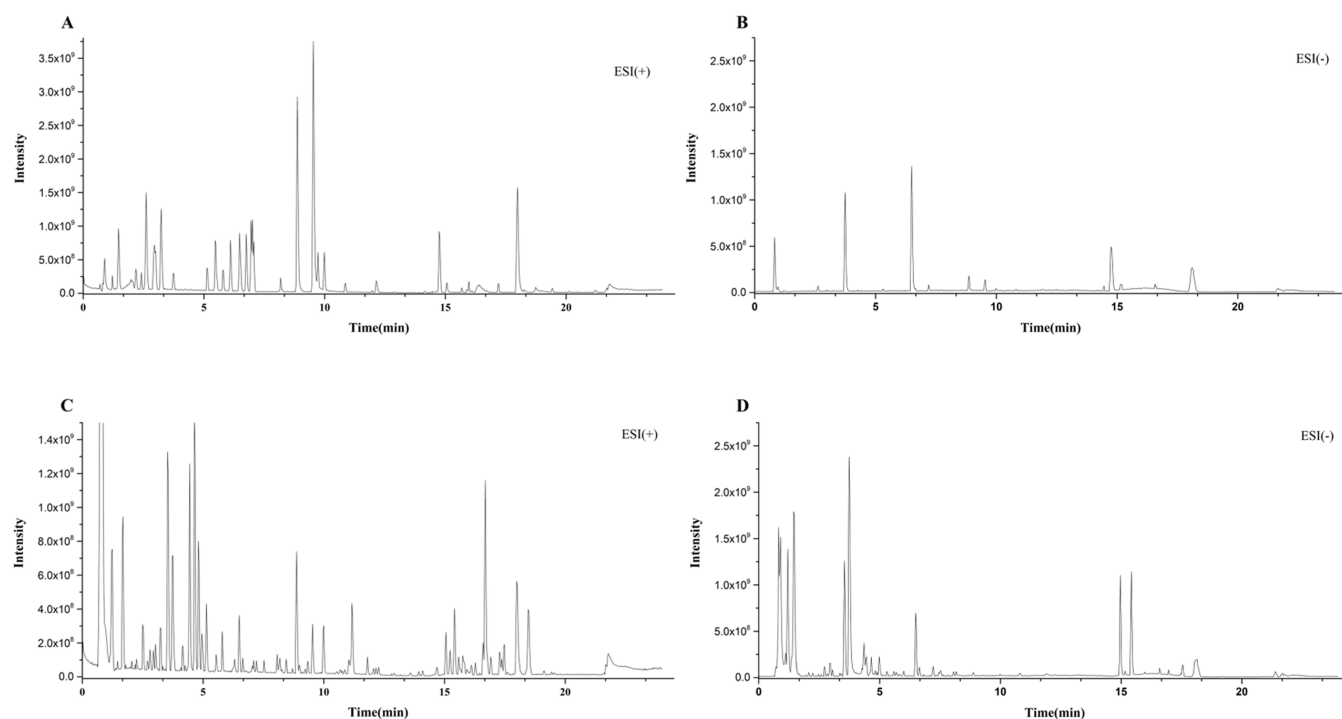
Figure 1. BPI chromatograms of mixed standard in positive (A) and negative (B) modes. BPI chromatograms of the ZWD water extracts were obtained in positive (C) and negative (D) modes.

then using the Cytoscape software for topology analysis. The specific process is as follows: (1) upload all of the above-mentioned common targets to the string platform, and set the source as the "Homo Sapiens"; (2) download the TSV format document, and import it into Cytoscape software (3.9.1) for data analysis; (3) use "Network Analyzer" plug-in to analyze the topology of the PPI network. The interaction network of ZWD in the treatment of HF target proteins was constructed.

2.8.4. Hub Gene Analysis. CytoHubba,[20] a plug-in Cytoscape, was applied to analyze the nodes in the PPI network of overlapping targets by the Maximal Clique Centrality (MCC) algorithm, which shows a better performance on the precision.[21] The parameters were set as the top = 5 nodes and were ranked by the MCC score.

2.8.5. GO Bioanalysis and KEGG Pathway Analysis. To clarify the function of the targets and their functions in signaling transduction, the DAVID 2021 database was applied to analyze the gene ontology (GO) and Kyoto Encyclopedia of Genes and Genomes (KEGG) pathway enrichment of the targets of ZWD against HF. GO enrichment analysis, including biological process (BP), cellular component (CC), and molecular function (MF), was performed. The enrichment degree of the core pathway was analyzed according to the *p*-value, and the possible mechanism of ZWD against HF was explored. Then, the results were presented in the form of a histogram (GO) and an advanced bubble chart (KEGG) with the help of bioinformatics (http://www.bioinformatics.com.cn/).

2.9. Molecular Docking Simulation. The protein crystal structure of the targets was obtained from RCSB Protein Data Bank (https://www.pdbus.org/) by downloading pdb format files. The water and ligand molecules were removed from the protein crystal structure using PyMOL software. The mol2 documents of SMCs were performed by energy minimization calculation using Chem 3D software. Then, both proteins and ligands were added with hydrogen using Autodock Tools 1.5.7 and were saved as Pdbqt files. The docking process was performed using AutoDock Vina to analyze the binding properties of the ligands for each protein. Proteins with lower binding energies were considered potential targets in HF treatment. Ligands with the lowest binding energy were selected for binding mode analysis. The visualization of the 3D binding model was performed by PyMOL.

2.10. Western Blot. The heart tissues were homogenized in RIPA lysis buffer, and the lysates were centrifuged at 3,000*g* and 4 °C for 10 min. Then, supernatants were collected and protein concentrations were determined using the BCA protein kit. Western blotting was performed following a standard protocol[22] and the blots were incubated with primary antibodies such as rabbit anti-p38 (1:1000), p-p38 (1:1000), JNK (1:1000), p-JNK (1:1000,), ERK (1:1000), p-ERK (1:2000), STAT3 (1:1000), and p-STAT3 (1:1000). Immunoblots were visualized with the ECL Western blot detection kit and quantified using ImageJ software (National Institutes of Health).

2.11. Statistical Analysis. The statistical significance of the data between groups was acquired using either Student's *t* test (for two groups) or one-way ANOVA multiple comparisons in GraphPad Pro 7.0 (GraphPad, San Diego, CA). *P* values <0.05 (*P* < 0.05) were considered statistically significant. All experiments were repeated at least three times.

3. RESULTS AND DISCUSSION

3.1. Identification and Classification of Chemical Constituents of Zhenwu Decoction. A total of 115 compounds were tentatively identified in ZWD, including 28 alkaloid compounds, 20 monoterpenoid glycosides, 10 sesquiterpenoid compounds, 16 triterpenoid compounds, 10 gingerol compounds, 13 organic acids, and 18 other types of compounds. Among them, 13 compounds were unambigu-

ously identified compared with the reference standards. The base peak ion (BPI) chromatograms of ZWD in the positive and negative ion modes are shown in Figure 1. Table S2 summarizes the accurate mass measurements (<5 ppm) for the protonated molecular ions of the 115 constituents in ZWD. Retention times, formulas, experimental and theoretical masses, mDa, and ppm errors were included.

3.1.1. Alkaloid Compounds. Twenty-eight alkaloid compounds were putatively identified from *Aconitum carmichaelii* Debx., which often share a C_{19} or C_{20} diterpenoid skeleton except Compounds 1 and 17.[23,24] Compound 17 displayed a $[M + H]^+$ ion at *m/z* 272.1286; the molecular formula was conjectured to $C_{16}H_{17}NO_3$, and four major corresponding fragment ions were observed at *m/z* 272.12812 $[M + H]^+$, 255.1017 $[M+H-NH_3]^+$, 161.0598 $[C_{10}H_9O_2]^+$, and 107.0496 $[C_7H_7O]^+$. The pattern of ion fragments was consistent with the reference standard. Thus, compound 17 was identified as higenamine.[25] Compound 1 was identified as salsolinol by a similar method. The other diterpenoid alkaloids often share a similar mass fragmentation behavior due to the same skeleton by losing neutral fragment molecules, such as CH_3COOH, CH_3OH, H_2O, $C_7H_6O_2$, *etc.* For instance, Compound 78 displayed a $[M + H]^+$ ion at *m/z* 616.3118, and further yielded the fragment ions at 556.2903 $[M+H-CH_3COOH]^+$, 524.2650 $[M+H-CH_3COOH-CH_3OH]^+$, 496.2690 $[M+H-CH_3COOH-CH_3OH-CO]^+$, 492.2379 $[M+H-CH_3COOH-CH_3OH \times 2]^+$, 464.2428 $[M+H-CH_3COOH-CH_3OH-CO \times 2]^+$, 338.1753 $[M+H-CH_3COOH-CH_3OH \times 3-C_7H_6O_2]^+$, and 105.03340 $[C_7H_5O]^+$. All of these data fit well with the reference standard, so compound 78 was unequivocally identified as hypaconitine. Similarly, compounds 62, 66, and 71 were identified as benzoylmesaconine, benzoylaconine, and benzoylhypaconine, respectively. The quasimolecular ion of compound 38 was observed at *m/z* 422.2904($C_{24}H_{39}NO_5$); the MS/MS spectrum contained ions including 422.2903 $[M + H]^+$, 390.2639 $[M+H-CH_3OH]^+$, 372.2537 $[M+H-CH_3OH-H_2O]^+$, and 358.2381 $[M+H-CH_3OH \times 2]^+$. Thus, compound 38 could be identified as talatisamine according to the literature.[23,26] The remaining compounds were identified by a similar method, and the proposed fragmentation mechanism of compound 38 is shown in Figure S1A.

3.1.2. Monoterpene Glycosides. Monoterpenoid glycosides with "cage-like" pinane skeleton are representative and main bioactive constituents in Paeoniae Radix Alba.[27] Loss of moiety at the C_8 position of pinane skeleton (M8), CH_2O, and $C_{10}H_{12}O_4$ was often observed in the MS/MS spectrum. In this case, 20 monoterpenoid glycosides were tentatively identified in ZWD. For example, compound 40 displayed $[M-H]^-$ and $[M+HCOO]^-$ ions at *m/z* 479.1566 ($C_{23}H_{28}O_{11}$) and 525.1618, respectively; further, MS/MS spectrum showed ions at *m/z* 449.1457 $[M-H-CH_2O]^-$ and 327.1090 $[M-H-CH_2O-M8]^-$. The fragment pattern was consistent with the reference standard. Therefore, compound 40 was identified as paeoniflorin. In the same way, compound 75 was identified as benzoylpaeoniflorin. Compound 21 displayed the $[M-H]^-$ ion at *m/z* 495.1518 ($C_{23}H_{28}O_{12}$), which contains one more oxygen atom than compound 40, and further yielded the fragment ions at 465.1407 $[M-H-CH_2O]^-$, 299.0804 $[M-H-C_{10}H_{12}O_4]^-$, and 165.0554 $[C_9H_9O_3]^-$. Based on the MS/MS spectrum, compound 21 could be identified as oxypaeoniflorin according to the literature, and the proposed fragmentation mechanism of compound 21 is shown in Figure S1B.

3.1.3. Sesquiterpenoid Lactones. Sesquiterpene lactones including atractylenolide I, atractylenolide II, and atractylenolide III are the major active compounds existing in Atractylodis Macrocephalae Rhizoma, which normally show strong signals in positive ion mode. The fragmentation behaviors mainly occurred in the lactonic ring and produced plenty of complex mass fragments such as $[M+H-H_2O]^+$, $[M+H-H_2O-CO]^+$, $[M+H-H_2O-C_3H_6]^+$, $[M+H-H_2O-C_5H_8]^+$, *etc.* For example, compound 86 displayed $[M + H]^+$ ion at *m/z* 249.1486, and product ions at 231.1381 $[M+H-H_2O]^+$, 203.1429 $[M+H-H_2O-CO]^+$, 189.0911 $[M+H-H_2O-C_3H_6]^+$, 175.0757 $[M+H-H_2O-C_3H_6-CH_2]^+$, 163.0755 $[M+H-H_2O-C_5H_8]^+$, and 119.0856 $[M+H-H_2O-C_5H_8-CO_2]^+$. After being compared with the MS/MS spectrum of the reference standard and the published literature,[28] compound 86 was ultimately identified as atractylenolide III; the proposed fragmentation mechanism is shown in Figure S1C. Similarly, components 96 and 105 were identified as atractylenolide II and atractylenolide I, respectively. Totally, 10 sesquiterpene lactones were tentatively identified.

3.1.4. Triterpenoid Compounds. Sixteen triterpenoid compounds were tentatively identified in ZWD and mainly belong to the lanostane type, which are classified into two categories according to the skeleton. One is closed-loop type and the other is split-ring type. Each type is divided into two subtypes according to the position of the double bond on the side chain of the substituent at C_{17}. Compound 93 exhibited the quasimolecular ion $[M-H]^-$ at *m/z* 497.3285 ($C_{31}H_{46}O_5$), and $[M-H+HCOO+Na]^-$ at *m/z* 565.3161; fragment ions such as 479.3198 $[M-H-H_2O]^-$, 419.2970 $[M-H-H_2O-CO_2-CH_4]^-$, and 403.2675 $[M-H-H_2O-CO_2-CH_4 \times 2]^-$ were observed. The fragment pathway was consistent with the report.[29] Therefore, compound 93 was tentatively identified as poricoic acid BM and the possible fragmentation pathway is exhibited in Figure S1D.

3.1.5. Gingerols and Shogaols. Gingerols and shogaols are active constituents that can be found in fresh ginger. Structurally, gingerols and shogaols share the same skeleton, but gingerols have a hydroxy while shogaols have a double bond at C_5 position instead. In this case, 10 gingerols and shogaols were tentatively identified by the protonated molecular ions $[M + H]^+$, the H_2O-subtracted protonated molecular ion $[M+H-H_2O]^+$, adduct ions $[M + Na]^+$, and characteristic fragment ions. For example, compound 84 displayed ions at *m/z* 295.1909 $[M + H]^+$, 277.1803 $[M+H-H_2O]^+$, and 317.1729 $[M + Na]^+$; positive ion fragments such as 277.1800 $[M+H-H_2O]^+$, 163.0755 $[C_{10}H_{11}O_2]^+$, and, especially, 137.0599 $[C_8H_9O_2]^+$, which was a characteristic fragment ion, were also found in the MS/MS spectrum. These ion patterns were consistent with the reference standard. Therefore, compound 84 was certainly identified as 6-gingerol and the presumed fragmentation mechanism is shown in Figure S1E. Similarly, 4-, 6-, 8-, and 10-shogaols were tentatively identified according to the mass patterns and literature information.[30]

3.1.6. Organic Acids. Organic acids are the most common chemical substances that are distributed in most of the herbs, and the origin of organic acids in ZWD might include all five herbs. Thirteen organic acids were tentatively identified in ZWD. For instance, compound 23 exhibited $[M + H]^+$ ion at *m/z* 355.1030 and $[M-H]^-$ ion at *m/z* 353.0883($C_{16}H_{18}O_9$). In the positive model, it lost the quinate and formed the ion of $[C_9H_9O_4]^+$ at 181.0492 and $[C_9H_9O_4-H_2O]^+$ at *m/z*
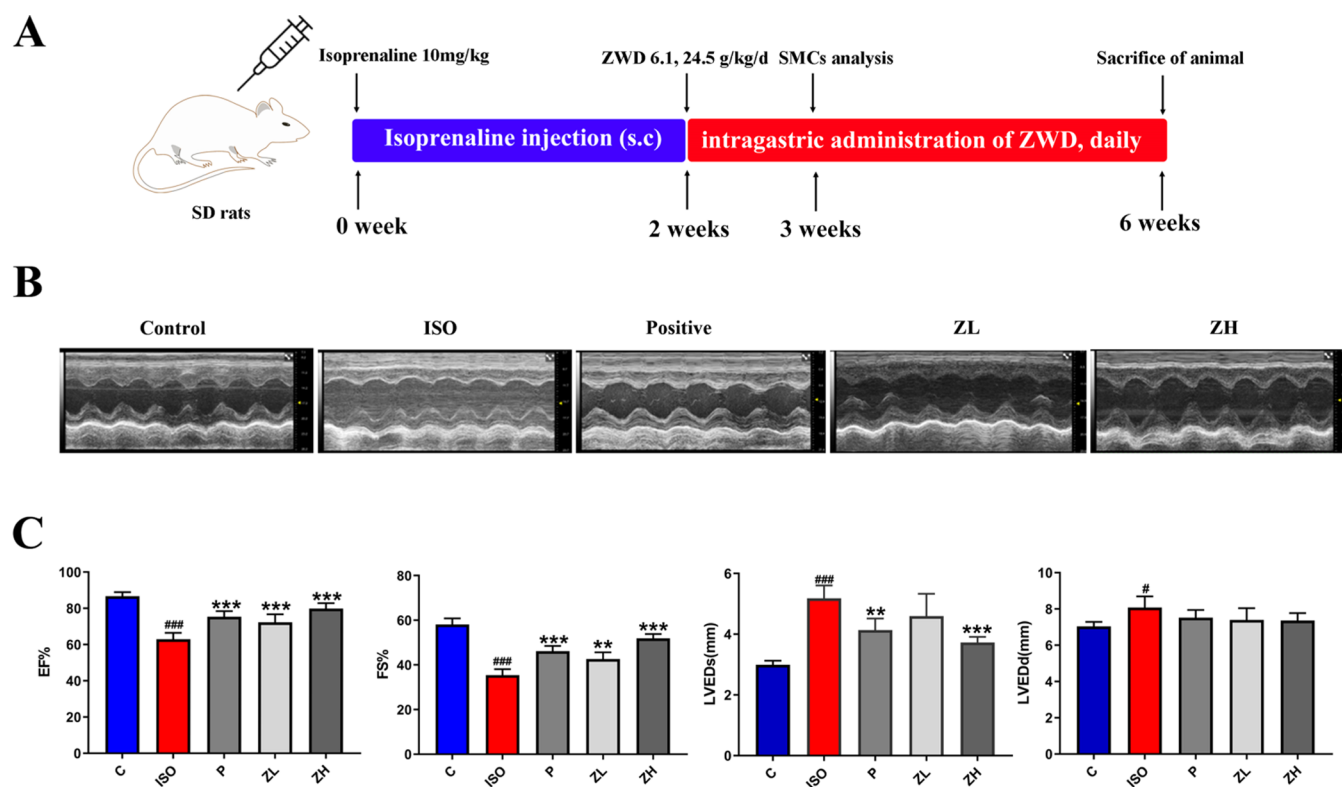
Figure 2. ZWD recovers cardiac function in ISO-induced heart failure. (A) Experimental design for an *in vivo* cardioprotective study of ZWD in HF rats. (B) Representative images of echocardiography. (C) Changes in echocardiographic parameters (EF%, FS %, LVEDs, and LVEDd) in various groups. Data are presented as means ± SD, $n = 6$. $**P < 0.01$, $***P < 0.001$ compared with the ISO group; $\#P < 0.05$, $\#\#\#P < 0.001$ compared with the control group.
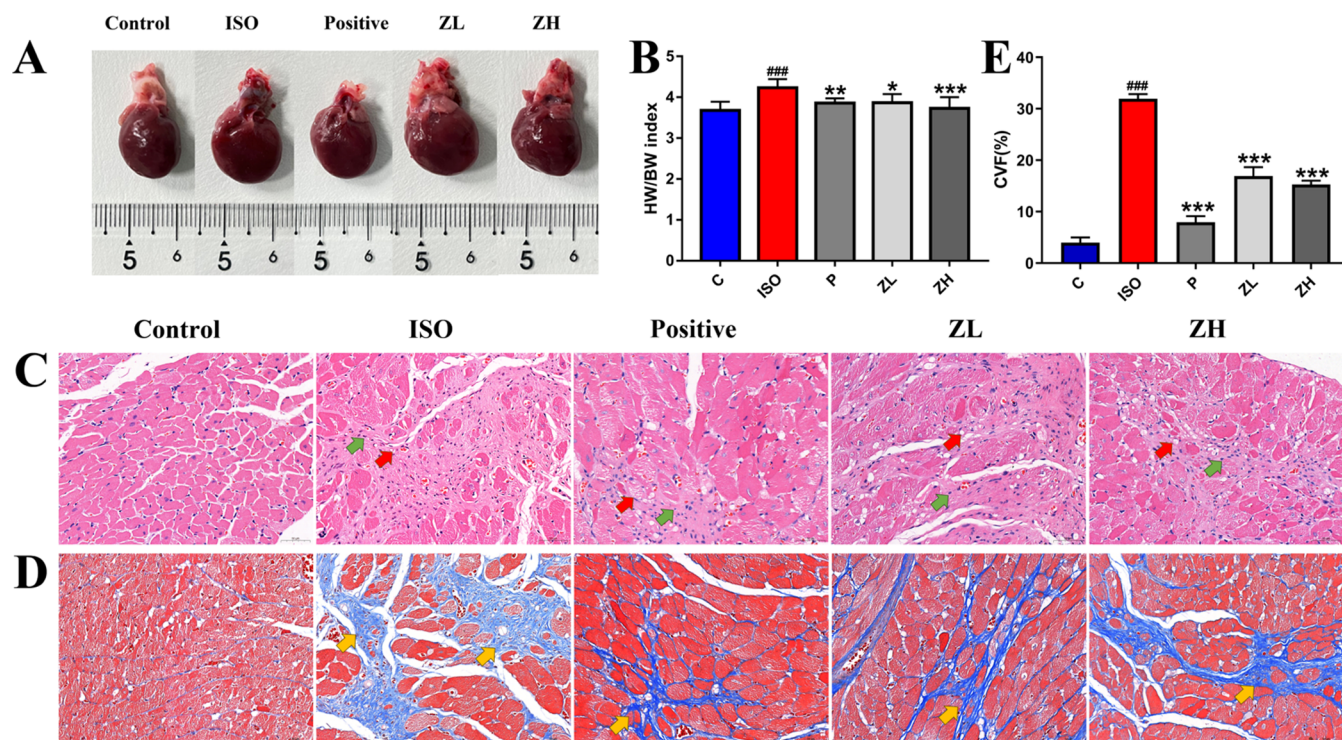

Figure 3. Therapeutic effects of ZWD in ISO-induced HF rats. (A) Representative images of gross hearts. (B) Ratio of the HW/BW index. (C) Representative images of HE staining results. (D) Representative images of Masson staining results. (E) Collagen volume fraction results of Masson staining. Heart tissues were visualized via a light microscope at ×400 magnification. Data are presented as means ± SD, $n = 3-8$. $*P < 0.05$, $**P < 0.01$, $***P < 0.001$, compared with the ISO group; $\#\#\#P < 0.001$, compared with the control group. Red, green, and yellow arrows stand for myocardial fiber necrosis, fibrocyte, and expression of myocardial fibers, respectively.
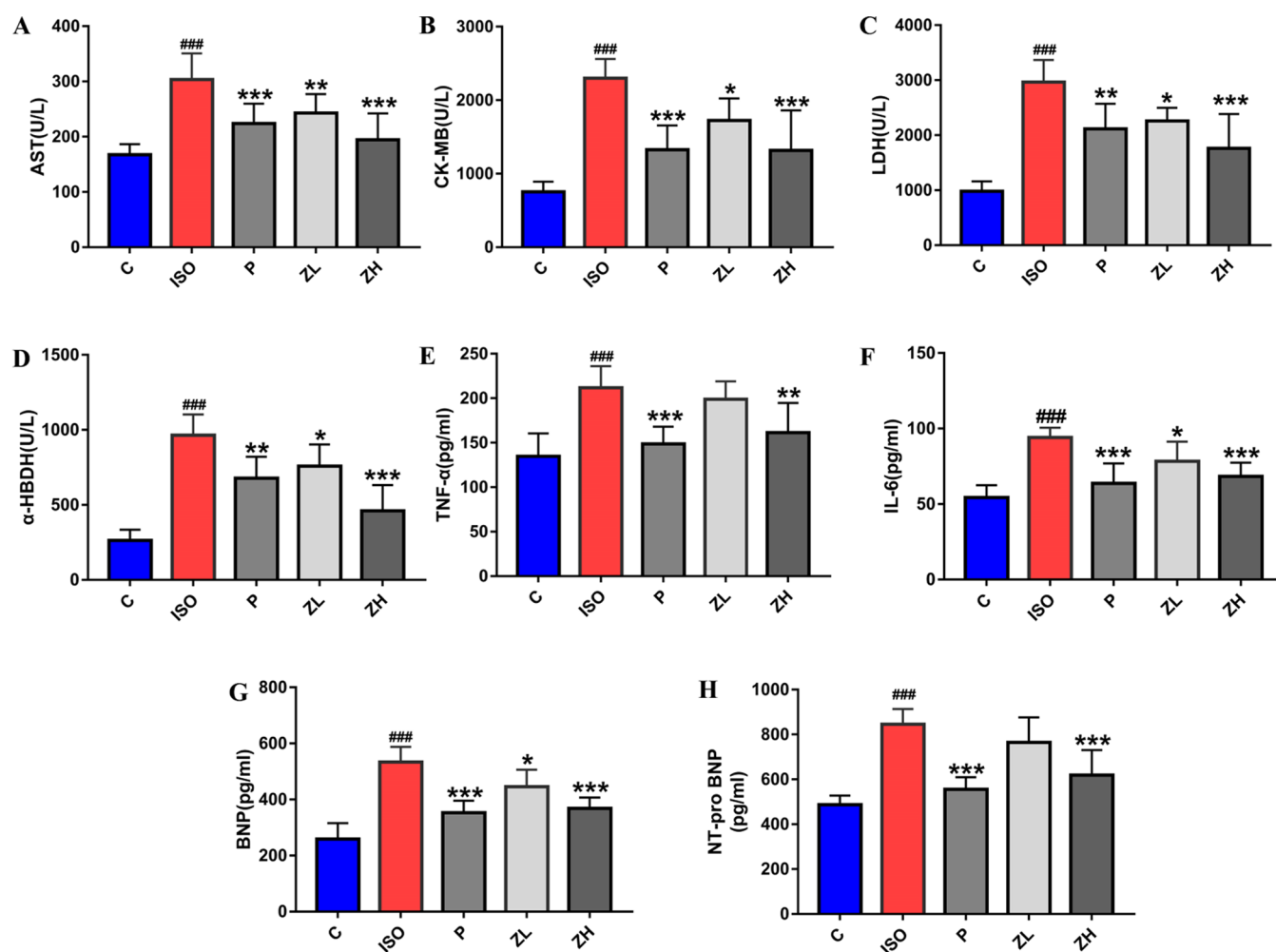
Figure 4. Analysis of serum biochemical indexes. (**A−H**) Serum levels of AST, CK-MB, LDH, α-HBDH, TNF-α, IL-6, BNP and NT-pro BNP. Data are presented as means ± SD, n = 8. $*P < 0.05$, $**P < 0.01$, $***P < 0.001$ compared with the ISO group, $^{###}P < 0.001$ compared with the control group.

163.0391. In the negative model, it lost the caffeic acid and formed the base peak of $[C_7H_{11}O_6]^-$ at m/z 191.0559. Thus, compound 23 could be tentatively identified as chlorogenic acid according to the published data.[31]

3.1.7. Other Compounds. Eighteen uncategorized compounds including flavonoids, coumarins, sugars, and fatty acid were also identified in ZWD. Compound 54 exhibited the $[M + H]^+$ ion at m/z 193.0498 and possessed the predicted molecular formula $C_{10}H_8O_4$. In the MS/MS spectrum, 193.0497 $[M + H]^+$, 178.0261 $[M+H−CH_3]^+$, 165.0548 $[M +H−CO]^+$, 150.0314 $[M+H−CO−CH_3]^+$, 133.0826 $[M+H− CH_3OH−CO]^+$, 122.0366 $[M+H−CO \times 2\text{-}CH_3]^+$, and 105.0340 $[M+H−CH_3OH−CO \times 2]^+$ were observed. The ion fragments were consistent with the mz Cloud, mz Vault database, and literature;[28] thus, compound 54 was tentatively identified as scopoletin.

3.2. Zhenwu Decoction Improved the Cardiac Function of Isoprenaline-Induced Heart Failure Rats.

3.2.1. Echocardiography. As shown in Figure 2C, compared with the control group, injection of ISO significantly reduced EF % ($P < 0.001$) and FS % ($P < 0.001$) and increased LVEDs ($P < 0.001$) and LVEDd ($P < 0.05$) in the HF rats. After 4 weeks of treatment, EF % and FS % were obviously elevated by high-dose ZWD treatment ($P < 0.001$). In contrast, high-dose

ZWD treatment obviously attenuated the elevation of the LVEDs in ISO-induced HF rats ($P < 0.001$). These results preliminarily demonstrated that ZWD improved the cardiac function and enhanced the capacity to withstand HF stress induced by ISO.

3.2.2. HW/BW Index and Histology Examination. Both low- and high-dose ZWD treatment could significantly attenuate myocardial hypertrophy and reduce the HW/BW index compared to the ISO group (Figure 3A,3B, $P < 0.05$, $P < 0.001$). HE staining showed that pathological changes such as myocardial fiber necrosis, fibrous tissue hyperplasia, and mast cell increase were observed in the cardiac tissue of rats of the ISO group (Figure 3D). However, ZWD treatment alleviated the pathological changes to a certain extent. Additionally, Masson staining results showed that CVF% in the ISO group was markedly higher than that in the control group, with a significant difference ($P < 0.001$), suggesting that a significant fibrous tissue hyperplasia occurred in the ISO group. Compared with the ISO group, CVF% was markedly reduced in the ZWD groups, with a significant difference (Figure 3E). The results illustrated that the ZWD protected the rats against ISO-induced myocardial injury and left ventricular hypertrophy.
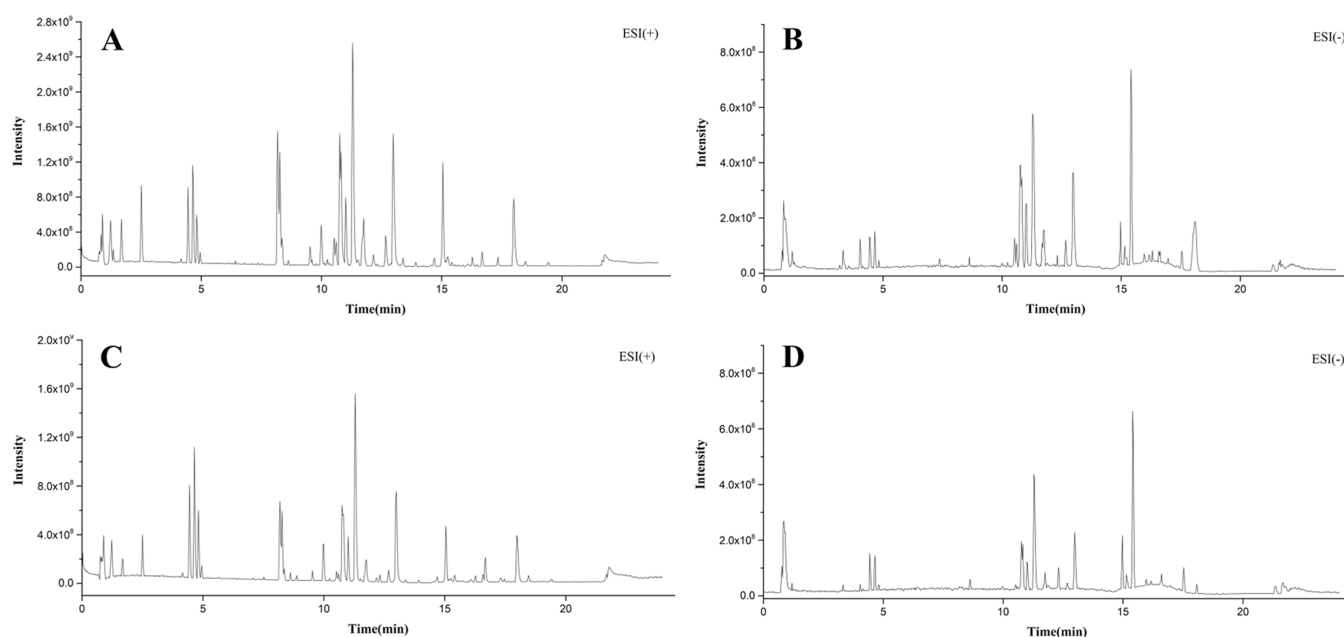
Figure 5. BPI chromatograms of the drug-containing serum in positive (A) and negative (B) modes. BPI chromatograms of the blank rat serum were obtained in positive (C) and negative (D) modes.
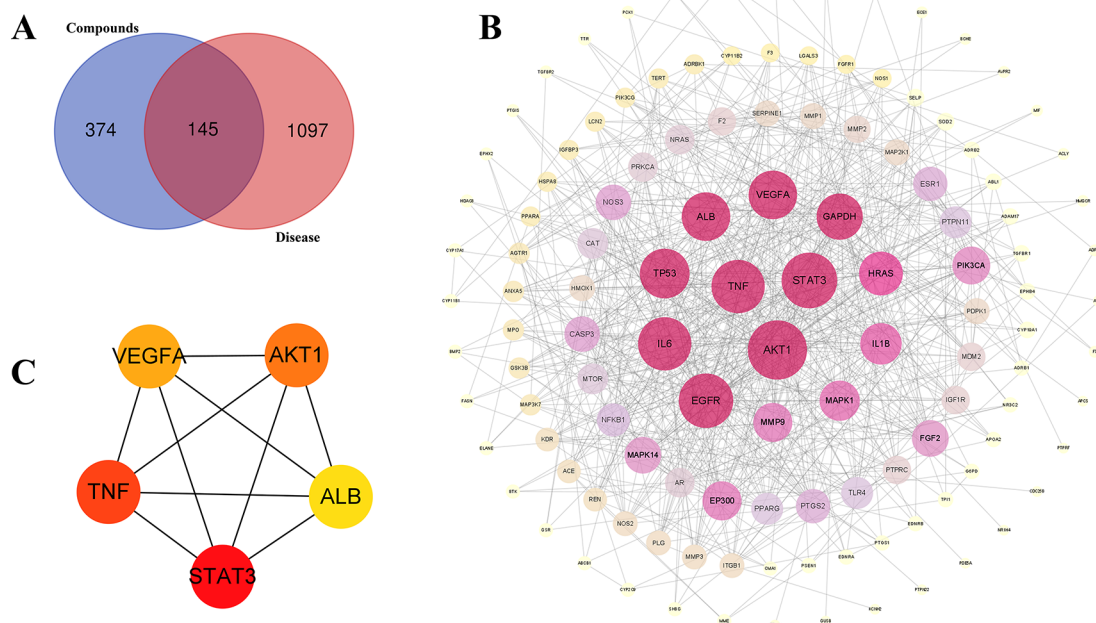

Figure 6. Results of common target screening, PPI network construction, and hub gene identification. (A) Venn diagram of chemical composition targets of ZWD and heart failure targets. Among them, the blue circle indicates that there are 519 chemical composition targets of ZWD, the orange circle represents 1242 heart failure targets, and the middle crossing part indicates 145 "common targets". (B) PPI network of the potential targets. Node size from large to small represents the descending order of the degree value. (C) The 5 hub genes identified from the PPI network.

3.2.3. Serum Biochemical Indexes Assessment. Biomarkers such as AST, CK-MB, LDH, and α-HBDH have been used for diagnosing myocardial injury.[32] When myocardially injured, AST, CK-MB, LDH, and α-HBDH will be released into the bloodstream. Increased levels of TNF-α and IL-6 have been described repeatedly in patients with chronic heart failure, showing a positive correlation with disease severity.[33] BNP and NT-pro BNP are well-known markers of heart failure for the detection of left ventricular hypertrophy and left ventricular

systolic dysfunction.[34,35] The serum levels of BNP and NT-pro BNP will increase in chronic congestive heart failure. ISO treatment induces myocardial injury, which may ultimately lead to myocardial necrosis, left ventricular hypertrophy, and heart failure.[36] In this study, a significant increase of the above biomarkers was detected in the ISO group, while decreased serum expression of these biomarkers was found in the positive control group and ZWD groups (Figure 4). The results further illustrated that the water extracts of ZWD protected the rats
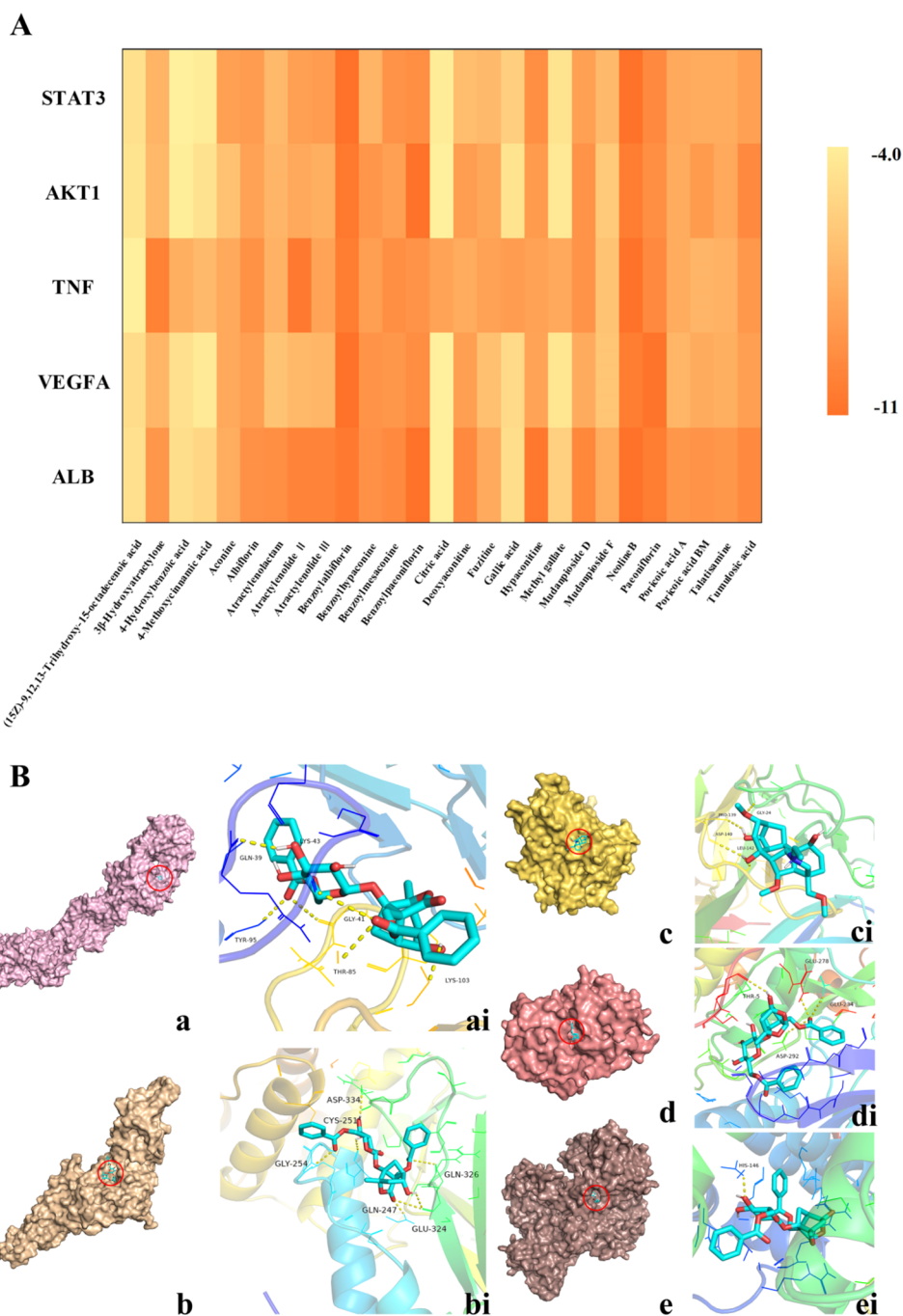
Figure 7. GO and KEGG pathway enrichment analysis results. (A) BP enrichment analysis (green bars); CC enrichment analysis (brown bars); and MF enrichment analysis (blue bars). (B) KEGG enrichment analysis. The size of each node indicates enriched counts; the abscissa represents the enriched gene ratio, and color indicates enriched adjusted P-value.

Figure 8. (A) Heat maps of the docking scores of hub genes combined with SMCs in ZWD. The ordinate represents the top five hub genes, and the abscissa represents the SMCs. (B) Molecular docking simulation of bioactive compound-hub genes. The illustration marked with a lowercase letter indicates the docking state between small-molecule compounds and large-molecule proteins, and the detailed docking condition on the right side (marked with lowercase letters with an "i") can be observed. (a) Benzoylalbiflorin to VEGFA (docking score = −9.5); (b) benzoylalbiflorin to STAT3 (docking score = −8.1); (c) neoline to TNF (docking score = −8.1); (d) benzoylpaeoniflorin to AKT1 (docking score = −10.7); (e) benzoylpaeoniflorin to ALB (docking score = −9.4).

against ISO-induced myocardial injury and left ventricular hypertrophy.

3.3. Identification of Serum Migrant Components of ZWD. Based on the results in section 3.1, a total of 33 prototype compounds was found and identified in serum after oral administration of ZWD. These compounds involved monoterpene glycosides, alkaloids, terpenoids, and organic acids such as paeoniflorin, benzoylmesaconine, atractylenolide III, *etc*. These SMCs were considered as bioactive compounds

and are marked with a "#" in Table S2. The BPI chromatograms of blank rat serum and drug-containing serum in the positive and negative ion modes are shown in Figure 5.

3.4. Network Construction of Zhenwu Decoction against Heart Failure based on Serum Migrant Components. *3.4.1. Retrieval Target Proteins of Bioactive Compounds.* The 33 prototype compounds absorbed in rat serum were considered as bioactive compounds. The structure information on six compounds was not found in Pubchem or
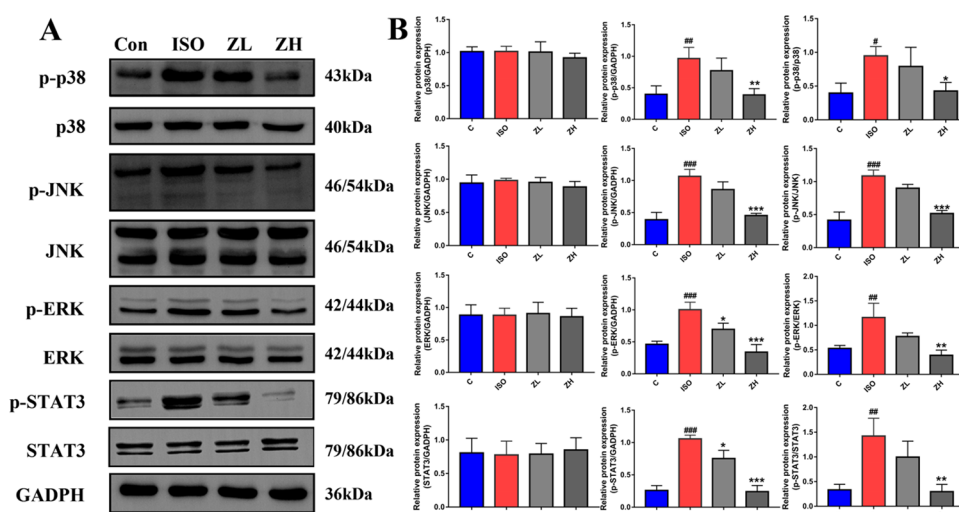
Figure 9. (A) Western blot bands showing the protein expression levels of signaling pathway proteins (total and phosphorylation of p38, JNK, ERK, and STAT3). (B) Relative protein expression for total and phosphorylation of p38, JNK, ERK, STAT3, and GAPDH were quantified by densitometry based on immunoblot images ($n = 3$). Values are presented as means $\pm$ SD. $*P < 0.05$, $**P < 0.01$, $***P < 0.001$ compared with the ISO group; $^{\#}P < 0.05$, $^{\#\#}P < 0.01$, $^{\#\#\#}P < 0.001$ compared with the control group.

other databases; therefore, 27 compounds were finally involved in the subsequent network study. Using PharmMapper, Swiss target predict, and TCMSP platform, we predicted the potential targets of the bioactive compounds. After removal of the duplicates, a total of 519 target genes was obtained.

3.4.2. Retrieval Target Proteins of Heart Failure. Using "Heart failure" as the keyword, 1204 targets were found in Gene Cards, 524 targets in OMIM, 131 targets in CTD, and 77 targets in TTD. Then, they were transformed into standard gene targets with "Homo sapiens" by the UniProtKB search function of the Uniprot database. After data integration and deduplication, a total of 1242 disease targets was obtained.

The chemical composition-related targets and disease targets obtained above were uploaded to draw a Venn diagram for analysis, and 145 potential target genes of the absorbed components for the treatment of HF were obtained (Figure 6A).

3.4.3. Serum Migrant Components—Target Network Construction. An SMC-target network was constructed to elucidate the relationship between the bioactive compounds of ZWD and their predicted targets (Figure S2). This network consisted of 172 nodes and 596 interaction edges, suggesting that ZWD acts on the entire systematic biological network system through multicompounds and multitargets. Among these compounds, paeoniflorin (degree 55) and albiflorin (degree 53) have the largest number of potential targets, along with mudanpioside D (degree 49), benzoylpaeoniflorin (degree 49), and benzoylalbiflorin (degree 47), indicating that these bioactive compounds with high degree values could play a more important role in the ZWD treating of HF.

3.4.4. Protein—Protein Interaction Network Construction and Hub Genes Analysis. The 145 common targets obtained from section 3.4.2 were uploaded to the String database. The targets with a confidence value greater than 0.7 were screened out and then imported into Cytoscape for network construction. Figure 6B gives a whole view of the relationships within 122 targets (the other 23 disconnected genes were excluded), which includes 122 nodes and 683 edges. Using the CytoHubba tool, the top 5 genes (STAT3, TNF, AKT1,

VEGFA, ALB) were screened out and considered as the hub genes (Figure 6C).

3.4.5. GO and KEGG Enrichment Analysis. To decipher the cardioprotective function of the potential targets, we performed GO and KEGG pathway enrichment analyses using DAVID 2021. The GO enrichment analysis showed that the biological processes related to the treatment of HF were mainly involved in the regulation of the response to drug, response to hypoxia, and the positive regulation of MAPK activity. In terms of cellular components, the plasma membrane, membrane raft, and integral component of plasma membrane were mainly involved, whereas in terms of molecular functions, the treatment of HF was mainly affected by endopeptidase activity, heme binding, and enzyme binding (Figure 7A). The results of the KEGG pathway enrichment analysis showed that the pathways were closely related to the PI3K-AKT, MAPK, and calcium signaling pathways and HIF-1, FoxO, IL-17, and VEGF signaling pathways (Figure 7B).

3.5. Molecular Docking Simulation. Molecular docking simulation was used to verify the binding ability between the SMCs of ZWD and the targets. A binding energy less than −4.25 kcal/mol indicated that the ligand molecule could certainly bind to the receptor target. A binding energy less than −5.0 and −7.0 kcal/mol indicated a good and strong binding ability, respectively.[37] According to Figure 8A (detailed data are listed in Table S3), most of the bioactive components of ZWD demonstrated good binding with the hub genes. Among them, albiflorin, benzoylalbiflorin, benzoylmesaconine, benzoylpaeoniflorin, mudanpioside D, neoline, and paeoniflorin exhibited a strong binding ability to all of the five hub genes, namely STAT3, TNF, AKT1, VEGFA, and ALB. This suggests that the ZWD had a strong potential as a therapeutic strategy for HF via these hub genes.

As shown in Figure 8B, the results showed that neoline had the strongest binding ability with TNF (docking score = −8.1), benzoylalbiflorin had the strongest binding ability with STAT3 (docking score = −8.1), and VEGFA (docking score = −9.5), benzoylpaeoniflorin had the strongest binding ability with AKT1 (docking score = −10.7) and ALB (docking score = −8.4). Considering "benzoylalbiflorin to STAT3" (Figure

8B(bi)) as an example, it was stabilized by six H-bonds with residues that included two glutamine amino acid residues (GLN-247 and GLN-236), a glycine amino acid residue (GLY-254), a glutamic amino acid residue (GLU-324), a cysteine amino acid residue (CYS-251), and an aspartic amino acid residue (ASP-334).

3.6. Zhenwu Decoction Improved the Cardiac Function of Induced Heart Failure Rats by Regulating STAT3/MAPK Pathways.

According to the target network pharmacology and molecular docking simulation results, the hub gene STAT3, AKT, PI3K/Akt, and MAPK pathways might be closely involved in the anti-HF effect of ZWD. We next used Western blot to determine the regulatory effect of ZWD on the STAT3/MAPK signaling pathway. As shown in Figure 9A, the phosphorylation levels of p38, JNK, ERK, and STAT3 were significantly increased in the ISO group compared with the control group, while they were reversed in the experimental groups. Meanwhile, statistical results showed that the ratios of p-p38/p38, p-JNK/JNK, p-ERK/ERK, and p-STAT3/STAT3 were significantly reduced after high-dose ZWD treatment (Figures 9B). These results suggested that ZWD can inhibit the activation of STAT3 and MAPK signaling pathways induced by ISO by inhibiting the phosphorylation of key proteins.

3.7. Discussion.

In this study, we used UHPLC-Q-Orbitrap-HRMS technology to identify the absorbed components of ZWD in HF rat serum and explore the possible effective components and their mechanisms for HF treatment using network pharmacology and experimental validation. The results comprehensively elaborated the chemical material basis of ZWD and provided an efficient and rapid analysis method for the qualitative analysis of chemical components in ZWD. This work undoubtedly will improve the quality control of ZWD.

ISO-induced cardiac hypertrophy is a reliable, reproducible, and well-characterized model associated with arrhythmias, cardiomyocyte loss, and fibrosis, with progression to heart failure.[38] We successfully established the ISO-induced HF model and found that ZWD could improve cardiac function and reduce serum biochemical indexes. Moreover, the disordered arrangement of myocardial fibers, muscle filament looseness, and fibrous tissue hyperplasia are significantly improved after ZWD intervention. The therapeutic value of high doses of ZWD is comparable to that of captopril. In short, these results indicate that ZWD can reduce heart injury caused by ISO via reverse cardiac hypertrophy and myocardial fibrosis. Based on the serum pharmacochemistry theory, the constituents absorbed into the blood after oral administration were considered the potential bioactive material basis of medicinal herbs.[14] Therefore, in this experiment, the ISO-induced HF rats were selected to study serum pharmacochemistry to better reflect the absorption of ZWD components under the pathological state of HF. We found that the SMCs of ZWD mainly came from Paeoniae Radix Alba, Atractylodis Macrocephalae Rhizome, Aconiti Lateralis Radix Preparata, and Poria, and we did not find absorbed prototype compounds from Zingiberis Rhizoma Recens. The possible explanation for this could be that compounds such as 6-gingerol were cleared very rapidly from the plasma with a short terminal half-life in rats. However, the metabolites of 6-gingerol may have a therapeutic effect because they at least stay in the body over 12 h after administration.[39] The undetectable compounds from Zingiberis Rhizoma Recens indicate that we should focus on metabolites in the subsequent research.

Through the network topology analysis of the SMCs-targets network and PPI network, we found that paeoniflorin, albiflorin, mudanpioside D, benzoylpaeoniflorin, and benzoylalbiflorin with a high degree value are the main potential active compounds of ZWD, and STAT3, TNF, AKT1, VEGFA, and ALB are the key targets of these SMCs. These key proteins are the core node of the PPI network, involved in the biological processes of immunity, inflammation, and angiogenesis in cardiac diseases.[40,41] The KEGG pathway enrichment analysis results showed that the predicted targets were closely related to the PI3K-AKT, MAPK, HIF-1, FoxO, IL-17, VEGF, and calcium signaling pathways. These pathways could be regulated by the SMCs of the ZWD and mediate various biological processes and cellular responses in the cardiac environment. Previous studies showed that the PI3K/AKT pathway activation is critical for cardiac hypertrophy and heart failure.[42] A recent study reported that ZWD could reduce cardiomyocyte apoptosis and myocardial pathological changes in HF rats by regulating the PI3K-AKT pathway,[43] which was consistent with the prediction results of our study. Finally, experimental validation was implemented according to our predicted results, using target network pharmacology. As expected, ZWD could improve cardiac function in HF rats by regulating the STAT3/MAPK pathways.

Paeoniflorin is the primary active component isolated from *Paeonia lactiflora* Pall, which could regulate the GPCR, MAPKs/NF-κB, PI3K/Akt/mTOR, JAK2/STAT3, and TGFβ/Smads pathways.[44] Paeoniflorin was also the highest content of the secondary metabolite ingredients in ZWD.[45] It is reported that paeoniflorin could attenuate cardiac hypertrophy, fibrosis, and inflammation and improve left ventricular function in spontaneously hypertensive rats by modulating the MAPK signaling pathway.[46] Albiflorin is the isomer of paeoniflorin, which could inhibit the MAPK/NF-κB pathways in the lungs of asthmatic mice.[47] Benzoylpaeoniflorin is a derivant of paeoniflorin, which could protect heart function and inhibit myocardial cell apoptosis in AMI model rats by promoting the Nrf2/HO-1 pathway.[48] However, the biological activities of mudanpioside D and benzoylalbiflorin were relatively less reported, and more investigation is needed in the future. Besides, the other SMCs, including water-soluble alkaloids (aconine, hypaconine, talatisamine, fuziline, and neoline), gallic acid, atractylenolide III, and atractylenolide II, have also been reported to play an essential role in improving cardiac function.[49−51]

STAT3 is a member of the STAT family and is dynamic in integrating multiple signaling pathways in several tissues.[52] Alterations in STAT3 activation and expression are associated with various pathophysiological adaptations in the heart, such as heart failure in humans and in a mouse model of dilated cardiomyopathy.[53−55] It is reported that the levels of phosphorylated STAT3 in HF rats were significantly increased, promoting the expression of downstream target NF-κB, a critical link in the inflammatory response, which can promote the release of IL-6 and TNF-α. IL-6 and TNF-α could lead to the aggravation of the body's inflammatory response, then accelerate myocardial injury, promote cardiomyocyte apoptosis, and finally aggravate HF.[56,57] In this study, the levels of IL-6 and TNF-α were remarkably decreased in the high-dose ZWD group, and the phosphorylation level of STAT3 was significantly reduced in the high-dose ZWD group compared

to the ISO group, indicating that ZWD could enhance the cardiac function of HF rats via suppressing the phosphorylation of STAT3.

MAPKs include four subfamilies, three of which have been well characterized: p38, JNK, and ERK.[58] Studies have demonstrated that p38 may be activated in the process of heart failure development, involved in the process of ventricular remodeling, and that inhibition of p38 is beneficial for the amelioration of ventricular remodeling.[59] JNK participates in signal transduction induced by various stressors, including autophagy and apoptosis, and the reduction of p-JNK is linked to the attenuation of cardiac remodeling. ERK is also distributed in various tissues and attends to the regulation of cell proliferation and differentiation.[60] Therefore, some investigators believe that inhibition of the MAPK pathway is necessary to alleviate pathological ventricular remodeling. In our study, the phosphorylation levels of p38, ERK, and JNK were significantly reduced in the high-dose ZWD group compared to the ISO group, while there were no significant changes in total proteins. We demonstrated that ZWD can significantly inhibit the expression of p-p38, p-JNK, p-ERK, and p-STAT3. Based on these results, we conclude that ZWD can alleviate ISO-induced heart failure by inhibiting the STAT3 and MAPK signaling pathways.

4. CONCLUSIONS

We present the first serum pharmacodynamic material-based study of ZWD in the HF rat model. The results suggested that the SMCs of ZWD may target multiple key proteins simultaneously and have multiple functional contributions to the main pathways, sequentially establishing a new balance in the biological system against HF. STAT3/MAPK pathways might be a potential mechanism of ZWD on HF, which requires further verification through in vitro experiments. Other signaling pathways predicted in our study should be investigated, and the potential active ingredients can be used to improve the quality control of ZWD.

■ ASSOCIATED CONTENT

ⓢ Supporting Information

The Supporting Information is available free of charge at https://pubs.acs.org/doi/10.1021/acsomega.3c05055.

Table S1. quantitative analysis results of the water extracts of ZWD by HPLC; Table S2. mass spectrometry qualitative results of ZWD by UHPLC-Q-Orbitrap-HRMS; Table S3. the docking scores of hub genes combining with SMCs in ZWD; Figure S1. the representative schematic maps of proposed fragmentation mechanism; Figure S2. SMCs - target network (PDF)

■ AUTHOR INFORMATION

Corresponding Authors

Chi Zhang − *Sichuan Engineering Technology Research Centre for Injection of Traditional Chinese Medicines, China Resources Sanjiu (Yaan) Pharmaceutical Co., Ltd., Yaan, Sichuan 625000, P. R. China*; Email: zhangchi46@999.com.cn

Li Wan − *State Key Laboratory of Southwestern Chinese Medicine Resources, School of pharmacy, Chengdu University of Traditional Chinese Medicine, Chengdu, Sichuan 611137,*

P. R. China; ⓞ orcid.org/0000-0003-2556-1827; Email: wanli@cdutcm.edu.cn

Authors

Ruiyu Li − *State Key Laboratory of Southwestern Chinese Medicine Resources, School of pharmacy, Chengdu University of Traditional Chinese Medicine, Chengdu, Sichuan 611137, P. R. China; Sichuan Engineering Technology Research Centre for Injection of Traditional Chinese Medicines, China Resources Sanjiu (Yaan) Pharmaceutical Co., Ltd., Yaan, Sichuan 625000, P. R. China;* ⓞ orcid.org/0009-0001-6401-0764

Lv Zhu − *State Key Laboratory of Southwestern Chinese Medicine Resources, School of pharmacy, Chengdu University of Traditional Chinese Medicine, Chengdu, Sichuan 611137, P. R. China*

Mengyao Wu − *State Key Laboratory of Southwestern Chinese Medicine Resources, School of pharmacy, Chengdu University of Traditional Chinese Medicine, Chengdu, Sichuan 611137, P. R. China*

Chengtian Tao − *State Key Laboratory of Southwestern Chinese Medicine Resources, School of pharmacy, Chengdu University of Traditional Chinese Medicine, Chengdu, Sichuan 611137, P. R. China*

Yang Lu − *State Key Laboratory of Southwestern Chinese Medicine Resources, School of pharmacy, Chengdu University of Traditional Chinese Medicine, Chengdu, Sichuan 611137, P. R. China*

Yunyan Zhao − *State Key Laboratory of Southwestern Chinese Medicine Resources, School of pharmacy, Chengdu University of Traditional Chinese Medicine, Chengdu, Sichuan 611137, P. R. China*

Xiaofeng Jiang − *Sichuan Engineering Technology Research Centre for Injection of Traditional Chinese Medicines, China Resources Sanjiu (Yaan) Pharmaceutical Co., Ltd., Yaan, Sichuan 625000, P. R. China*

Complete contact information is available at:
https://pubs.acs.org/10.1021/acsomega.3c05055

Author Contributions

§R.L. and L.Z. contributed equally to this work.

Notes

The authors declare no competing financial interest.

■ ACKNOWLEDGMENTS

■ ABBREVIATIONS:

AST, aspartate aminotransferase; LDH, lactate dehydrogenase; CK-MB, creatine kinase isoenzymes; α-HBDH, α-hydroxybutyrate dehydrogenase; TNF-α, tumor necrosis factor-α; IL-6, interleukin-6; IL-17, interleukin-17; BNP, brain natriuretic peptide; NT-pro BNP, N-terminal pro-brain natriuretic peptide; VEGFA, vascular endothelial growth factor A; AKT1, serine/threonine kinase-1; ALB, albumin; STAT3, signal transducer and activator of transcription 3; MAPK, mitogen-activated protein kinase; JNK, c-Jun N-terminal kinase; ERK, extracellular signal-regulated kinase; HIF-1, hypoxia inducible factor-l; FoxO, forkhead box O; GPCR, G-protein-coupled receptors; NF-κB, nuclear factor-κB; PI3K,

phosphatidylinositol 3-hydroxy kinase; mTOR, mammalian target of rapamycin; JAK2, Janus kinase 2; TGFβ, Transforming growth factor-β; Smads, Drosophila mothers against decapentaplegic protein; Nrf2, nuclear factor erythroid 2-related factor 2; HO-1, heme oxygenase-1

■ REFERENCES

(1) Metra, M.; Teerlink, J. R. Heart failure. *Lancet* 2017, 390, 1981−1995.

(2) Savarese, G.; Lund, L. H Global Public Health Burden of Heart Failure. *Card. Fail. Rev.* 2017, 03, 7.

(3) Tham, Y. K.; Bernardo, B. C.; Ooi, J. Y. Y.; Weeks, K. L.; McMullen, J. R. Pathophysiology of cardiac hypertrophy and heart failure: signaling pathways and novel therapeutic targets. *Arch. Toxicol.* 2015, 89, 1401−1438.

(4) Zannad, F. Rising incidence of heart failure demands action. *Lancet* 2018, 391, 518−519.

(5) Li, X. M.; Ma, H. B.; Ma, Z. Q.; Li, L. F.; Xu, C. L.; Qu, R.; Ma, S. P. Ameliorative and neuroprotective effect in MPTP model of Parkinson's disease by Zhen-Wu-Tang (ZWT), a traditional Chinese medicine. *J. Ethnopharmacol.* 2010, 130, 19−27.

(6) Liang, C.-l.; Wu, J.; Lai, J.; Ye, S.; Lin, J.; Ouyang, H.; Zhan, J. Y.; Zhou, J. Protection Effect of Zhen-Wu-Tang on Adriamycin-Induced Nephrotic Syndrome via Inhibiting Oxidative Lesions and Inflammation Damage. *J. Evidence-Based Complementary Altern. Med.* 2014, 2014, 1−11.

(7) Liu, Q.; Hu, S.; He, Y.; Zhang, J.; Zeng, X.; Gong, F.; Liang, L. The protective effects of Zhen-Wu-Tang against cisplatin-induced acute kidney injury in rats. *PLoS One* 2017, 12, No. e0179137.

(8) Cai, Y.; Chen, J.; Jiang, J.; Cao, W.; He, L. Zhen-wu-tang, a blended traditional Chinese herbal medicine, ameliorates proteinuria and renal damage of streptozotocin-induced diabetic nephropathy in rats. *J. Ethnopharmacol.* 2010, 131, 88−94.

(9) Tang, Q.; Wang, Y.; Li, K. Zhenwu decoction for chronic heart failure Protocol for a systematic review and meta-analysis. *Medicine* 2018, 97, No. e11559.

(10) Wang, Y.; Fan, X.; Qu, H.; Gao, X.; Cheng, Y. Strategies and Techniques for Multi-Component Drug Design from Medicinal Herbs and Traditional Chinese Medicine. *Curr. Top. Med. Chem.* 2012, 12, 1356−1362.

(11) Matos, L. C.; Machado, J. P.; Monteiro, F. J.; Greten, H. J. Understanding Traditional Chinese Medicine Therapeutics: An Overview of the Basics and Clinical Applications. *Healthcare* 2021, 9, 257.

(12) Wang, M.; Liu, F.; Yao, Y.; Zhang, Q.; Lu, Z.; Zhang, R.; Liu, C.; Lin, C.; Zhu, C. Network pharmacology-based mechanism prediction and pharmacological validation of Xiaoyan Lidan formula on attenuating alpha-naphthylisothiocyanate induced cholestatic hepatic injury in rats. *J. Ethnopharmacol.* 2021, 270, No. 113816.

(13) Wei, J.; Yu, Y.; Zhang, Y.; Li, L.; Li, X.; Shao, J.; Li, Y. Integrated Serum Pharmacochemistry and Network Pharmacology Approach to Explore the Effective Components and Potential Mechanisms of Menispermi Rhizoma Against Myocardial Ischemia. *Front. Chem.* 2022, 10, No. 869972.

(14) Wang, X. J. Studies on serum pharmacochemistry of traditional Chinese medicine. *World. Sci. Technol.* 2002, 1−4.

(15) Gertsch, J. Botanical Drugs, Synergy, and Network Pharmacology: Forth and Back to Intelligent Mixtures. *Planta Med.* 2011, 77, 1086−1098.

(16) Al-Nesf, A.; Mohamed-Ali, N.; Acquaah, V.; Al-Jaber, M.; Al-Nesf, M.; Yassin, M. A.; Orie, N. N.; Voss, S. C.; Georgakopoulos, C.; Bhatt, R.; Beotra, A.; Mohamed-Ali, V.; Al-Maadheed, M. Untargeted Metabolomics Identifies a Novel Panel of Markers for Autologous Blood Transfusion. *Metabolites* 2022, 12, 425.

(17) Cai, W.; Li, K.; Xiong, P.; Gong, K.; Zhu, L.; Yang, J.; Wu, W. A systematic strategy for rapid identification of chlorogenic acids derivatives in Duhaldea nervosa using UHPLC-Q-Exactive Orbitrap mass spectrometry. *Arabian J. Chem.* 2020, 13, 3751−3761.

(18) Zhao, Y.; Cao, J.; Zhao, J.; Wei, P.; Wu, R.; Zhang, J.; Wan, L. Chemical analysis of Chrysosplenium from different species by UPLC-Q exactive orbitrap HRMS and HPLC-DAD. *J. Pharm. Biomed. Anal.* 2022, 218, No. 114861.

(19) Lv, L.; Wei, X.; Wang, M.; Zhang, X.; Ma, X.; Dorje, D.; Jia, S.; Qi, Y. Effects of Wenyang Yiqi Huoxue Prescription on Na^+-K^+-ATPase and Ca^{2+}-ATPase in Myocardial Tissue of Rats with Chronic Heart Failure. *Chin. J. Inf. Tradit. Chin. Med.* 2023, 30, 74−80.

(20) Chin, C. H.; Chen, S. H.; Wu, H. H.; Ho, C. W.; Ko, M. T.; Lin, C. Y. cytoHubba: identifying hub objects and sub-networks from complex interactome. *BMC Syst. Biol.* 2014, 8, S11.

(21) Xu, L.; Zhang, J.; Wang, Y.; Zhang, Z.; Wang, F.; Tang, X. Uncovering the mechanism of Ge-Gen-Qin-Lian decoction for treating ulcerative colitis based on network pharmacology and molecular docking verification. *Biosci. Rep.* 2021, 41, No. BSR20203565.

(22) Gwozdz, T.; Dorey, K. *Basic Science Methods for Clinical Researchers*; Elsevier, 2017; pp 99−117.

(23) Hu, R.; Zhao, J.; Qi, L. W.; Li, P.; Jing, S. L.; Li, H. J. Structural characterization and identification of C_{19}- and C_{20}-diterpenoid alkaloids in roots of *Aconitum carmichaeli* by rapid-resolution liquid chromatography coupled with time-of-flight mass spectrometry: Alkaloids in *Aconitum carmichaeli* by RRLC/TOFMS. *Rapid Commun. Mass Spectrom.* 2009, 23, 1619−1635.

(24) Wang, B.; Dong, J.; Ji, J.; Yuan, J.; Wang, J.; Wu, J.; Tan, P.; Liu, Y. Study on the Alkaloids in Tibetan Medicine Aconitum pendulum Busch by HPLC−MSn Combined with Column Chromatography. *J. Chromatogr. Sci.* 2016, 54, 752−758.

(25) Zhao, X.; Yuan, Y.; Wei, H.; Fei, Q.; Luan, Z.; Wang, X.; Xu, Y.; Lu, J. Identification and characterization of higenamine metabolites in human urine by quadrupole-orbitrap LC-MS/MS for doping control. *J. Pharm. Biomed. Anal.* 2022, 214, No. 114732.

(26) Zhi, M.; Gu, X.; Han, S.; Liu, K.; Liu, Z.; Tang, Y.; Han, X.; Li, F.; Yang, Z.; Tan, P.; Zhao, H.; Du, H. Chemical variation in Aconti Kusnezoffii Radix before and after processing based on UPLC-Orbitrap-MS. *China J. Chin. Mater. Med.* 2020, 45, 1082−1089.

(27) Shi, Y.-H.; Zhu, S.; Ge, Y.; Toume, K.; Wang, Z.; Batkhuu, J.; Komatsu, K. Characterization and quantification of monoterpenoids in different types of peony root and the related Paeonia species by liquid chromatography coupled with ion trap and time-of-flight mass spectrometry. *J. Pharm. Biomed. Anal.* 2016, 129, 581−592.

(28) Xu, Y.; Cai, H.; Cao, G.; Duan, Y.; Pei, K.; Tu, S.; Zhou, J.; Xie, L.; Sun, D.; Zhao, J.; Liu, J.; Wang, X.; Shen, L. Profiling and Analysis of Multiple Constituents in Baizhu Shaoyao San before and after Processing by Stir-Frying Using UHPLC/Q-TOF-MS/MS Coupled with Multivariate Statistical Analysis. *J. Chromatogr. B* 2018, 1083, 110−123.

(29) Zou, Y.; Long, F.; Wu, C.; Zhou, J.; Zhang, W.; Xu, J.; Zhang, Y.; Li, S. A dereplication strategy for identifying triterpene acid analogues in *Poria cocos* by comparing predicted and acquired UPLC-ESI-QTOF-MS/MS data. *Phytochem. Anal.* 2019, 30, 292−310.

(30) Park, S. Y.; Jung, M. Y. UHPLC-ESI-MS/MS for the Quantification of Eight Major Gingerols and Shogaols in Ginger Products: Effects of Ionization Polarity and Mobile Phase Modifier on the Sensitivity. *J. Food Sci.* 2016, 81, C2457−C2465.

(31) Xu, H.; Niu, H.; He, B.; Cui, C.; Li, Q.; Bi, K. Comprehensive Qualitative Ingredient Profiling of Chinese Herbal Formula Wu-Zhu-Yu Decoction via a Mass Defect and Fragment Filtering Approach Using High Resolution Mass Spectrometry. *Molecules* 2016, 21, 664.

(32) Luan, F.; Rao, Z.; Peng, L.; Lei, Z.; Zeng, J.; Peng, X.; Yang, R.; Liu, R.; Zeng, N. Cinnamic acid preserves against myocardial ischemia/reperfusion injury via suppression of NLRP3/Caspase-1/GSDMD signaling pathway. *Phytomedicine* 2022, 100, No. 154047.

(33) Hedayat, M.; Mahmoudi, M. J.; Rose, N. R.; Rezaei, N. Proinflammatory cytokines in heart failure: double-edged swords. *Heart Failure Rev.* 2010, 15, 543−562.

(34) Sato, K.; Kumar, A.; Krishnaswamy, A.; Mick, S.; Desai, M. Y.; Griffin, B. P.; Kapadia, S. R.; Popović, Z. B. B-type natriuretic peptide is associated with remodeling and exercise capacity after transcatheter

aortic valve replacement for aortic stenosis. *Clin. Cardiol.* **2019**, *42*, 270−276.

(35) Smadja, D. M.; Fellous, B. A.; Bonnet, G.; Hauw-Berlemont, C.; Sutter, W.; Beauvais, A.; Fauvel, C.; Philippe, A.; Weizman, O.; Mika, D.; Juvin, P.; Waldmann, V.; Diehl, J.-L.; Cohen, A.; Chocron, R. D-dimer, BNP/NT-pro-BNP, and creatinine are reliable decision-making biomarkers in life-sustaining therapies withholding and withdrawing during COVID-19 outbreak. *Front. Cardiovasc. Med.* **2022**, *9*, No. 935333.

(36) Nichtova, Z.; Novotova, M.; Kralova, E.; Stankovicova, T. Morphological and functional characteristics of models of experimental myocardial injury induced by isoproterenol. *Gen. Physiol. Biophys.* **2012**, *31*, 141−151.

(37) Liu, J.; Liu, J.; Tong, X.; Peng, W.; Wei, S.; Sun, T.; Wang, Y.; Zhang, B.; Li, W. Network Pharmacology Prediction and Molecular Docking-Based Strategy to Discover the Potential Pharmacological Mechanism of Huai Hua San Against Ulcerative Colitis. *Drug Des., Dev. Ther.* **2021**, *Volume 15*, 3255−3276.

(38) Krenek, P.; Kmecova, J.; Kucerova, D.; Bajuszova, Z.; Musil, P.; Gazova, A.; Ochodnicky, P.; Klimas, J.; Kyselovic, J. Isoproterenol-induced heart failure in the rat is associated with nitric oxide-dependent functional alterations of cardiac function. *Eur. J. Heart Failure* **2009**, *11*, 140−146.

(39) Nakazawa, T.; Ohsawa, K. Metabolism of [6]-Gingerol in Rats. *Life Sci.* **2002**, *70* (18), 2165−2175.

(40) Kurdi, M.; Zgheib, C.; Booz, G. W. Recent Developments on the Crosstalk Between STAT3 and Inflammation in Heart Function and Disease. *Front. Immunol.* **2018**, *9*, 3029.

(41) Lal, N.; Puri, K.; Rodrigues, B. Vascular Endothelial Growth Factor B and Its Signaling. *Front. Cardiovasc. Med.* **2018**, *5*, 39.

(42) Aoyagi, T.; Matsui, T. Phosphoinositide-3 Kinase Signaling in Cardiac Hypertrophy and Heart Failure. *Curr. Pharm. Des.* **2011**, *17*, 1818−1824.

(43) Wang, X.; Chen, Z. Q.; Li, L.; Liao, J. H.; Wang, X. L.; Liu, J. Y.; Liao, D. H. Effect of Zhenwu decoction on cardiomyocyte apoptosis and the PI3K-AKT pathway in rats with congestive heart failure. *Chin. J. Comp. Med.* **2022**, *32*, 27−33.

(44) Zhang, L.; Wei, W. Anti-inflammatory and immunoregulatory effects of paeoniflorin and total glucosides of paeony. *Pharmacol. Ther.* **2020**, *207*, No. 107452.

(45) Tian, P.; Wei, H. C.; Han, D. E.; Jing, T. Y.; Ma, K. HPLC-ELSD fingerprint of Zhenwu Decoction and simultaneous determination of 13 components. *Chin. Tradit. Herb. Drugs* **2020**, *51*, 5980−5989.

(46) Liu, X.; Chen, K.; Zhuang, Y.; Huang, Y.; Sui, Y.; Zhang, Y.; Lv, L.; Zhang, G. Paeoniflorin improves pressure overload-induced cardiac remodeling by modulating the MAPK signaling pathway in spontaneously hypertensive rats. *Biomed. Pharmacother.* **2019**, *111*, 695−704.

(47) Cai, Z.; Liu, J.; Bian, H.; Cai, J. Albiflorin alleviates ovalbumin (OVA)-induced pulmonary inflammation in asthmatic mice. *Am. J. Transl. Res.* **2019**, *11*, 7300−7309.

(48) Yu, L.; Wu, Y. Effects of Benzoylpaeoniflorin on Cardiac Function in Rats with Myocardial Infarction via Promoting Nrf2 /HO-1 Pathway. *Lab. Anim. Sci.* **2022**, *39*, 44−48.

(49) Chen, Y.; Yang, W.; Guo, L.; Wu, X.; Zhang, T.; Liu, J.; Zhang, J. Atractylodes lactone compounds inhibit platelet activation. *Platelets* **2017**, *28*, 194−202.

(50) Xu, X.; Xie, X.; Zhang, H.; Wang, P.; Li, G.; Chen, J.; Chen, G.; Cao, X.; Xiong, L.; Peng, F.; Peng, C. Water-soluble alkaloids extracted from Aconiti Radix lateralis praeparata protect against chronic heart failure in rats via a calcium signaling pathway. *Biomed. Pharmacother.* **2021**, *135*, No. 111184.

(51) Yan, X.; Zhang, Y.-L.; Zhang, L.; Zou, L.-X.; Chen, C.; Liu, Y.; Xia, Y.-L.; Li, H.-H. Gallic Acid Suppresses Cardiac Hypertrophic Remodeling and Heart Failure. *Mol. Nutr. Food Res.* **2019**, *63*, No. 1800807.

(52) Zhang, W.; Qu, X.; Chen, B.; Snyder, M.; Wang, M.; Li, B.; Tang, Y.; Chen, H.; Zhu, W.; Zhan, L.; Yin, N.; Li, D.; Xie, L.; Liu, Y.; Zhang, J. J.; Fu, X.-Y.; Rubart, M.; Song, L.-S.; Huang, X.-Y.; Shou, W. Critical Roles of STAT3 in β-Adrenergic Functions in the Heart. *Circulation* **2016**, *133*, 48−61.

(53) Fischer, P.; Hilfiker-Kleiner, D. Survival pathways in hypertrophy and heart failure: the gp130-STAT3 axis. *Basic Res. Cardiol.* **2007**, *102*, 279−297.

(54) Ng, D. C. H.; Court, N. W.; dos Remedios, C. G.; Bogoyevitch, M. A. Activation of signal transducer and activator of transcription (STAT) pathways in failing human hearts. *Cardiovasc. Res.* **2003**, *57*, 333−346.

(55) Tsoutsman, T.; Kelly, M.; Ng, D. C. H.; Tan, J.-E.; Tu, E.; Lam, L.; Bogoyevitch, M. A.; Seidman, C. E.; Seidman, J. G.; Semsarian, C. Severe heart failure and early mortality in a double-mutation mouse model of familial hypertrophic cardiomyopathy. *Circulation* **2008**, *117*, 1820−1831.

(56) Van Linthout, S.; Tschöpe, C. Inflammation − Cause or Consequence of Heart Failure or Both? *Curr. Heart Failure Rep.* **2017**, *14*, 251−265.

(57) Markousis-Mavrogenis, G.; Tromp, J.; Ouwerkerk, W.; Devalaraja, M.; Anker, S. D.; Cleland, J. G.; Dickstein, K.; Filippatos, G. S.; van der Harst, P.; Lang, C. C.; Metra, M.; Ng, L. L.; Ponikowski, P.; Samani, N. J.; Zannad, F.; Zwinderman, A. H.; Hillege, H. L.; van Veldhuisen, D. J.; Kakkar, R.; Voors, A. A.; van der Meer, P. The clinical significance of interleukin-6 in heart failure: results from the BIOSTAT-CHF study. *Eur. J. Heart Failure* **2019**, *21*, 965−973.

(58) Gao, G.; Jiang, S.; Ge, L.; Zhang, S.; Zhai, C.; Chen, W.; Sui, S. Atorvastatin Improves Doxorubicin-Induced Cardiac Dysfunction by Modulating Hsp70, Akt, and MAPK Signaling Pathways. *J. Cardiovasc. Pharmacol.* **2019**, *73*, 223−231.

(59) Arabacilar, P.; Marber, M. The case for inhibiting p38 mitogen-activated protein kinase in heart failure. *Front. Pharmacol.* **2015**, *6*, No. 102, DOI: 10.3389/fphar.2015.00102.

(60) Wang, N.; Guan, P.; Zhang, J.-P.; Li, Y.-Q.; Chang, Y.-Z.; Shi, Z.-H.; Wang, F.-Y.; Chu, L. Fasudil hydrochloride hydrate, a Rho-kinase inhibitor, suppresses isoproterenol-induced heart failure in rats via JNK and ERK1/2 pathways. *J. Cell. Biochem.* **2011**, *112*, 1920−1929.